







Article

# Se··· $\pi$ Chalcogen Bonding in 1,2,4-Selenodiazolium Tetraphenylborate Complexes

Alexander A. Sapronov<sup>1</sup>, Alexey S. Kubasov<sup>2</sup>, Victor N. Khrustalev<sup>1,3</sup>, Alexey A. Artemjev<sup>1</sup>, Gleb M. Burkin<sup>1</sup>, Evgeny A. Dukhnovsky<sup>1</sup>, Alexander O. Chizhov<sup>3</sup>, Andreii S. Kritchenkov<sup>1</sup>, Rosa M. Gomila<sup>4</sup>, Antonio Frontera<sup>4</sup> and Alexander G. Tskhovrebov<sup>1,\*</sup>

<sup>1</sup> Research Institute of Chemistry, Peoples' Friendship University of Russia, 6 Miklukho-Maklaya Street, 117198 Moscow, Russia

<sup>2</sup> Kurnakov Institute of General and Inorganic Chemistry, Russian Academy of Sciences, Leninsky Prosp. 31, 119991 Moscow, Russia

<sup>3</sup> N.D. Zelinsky Institute of Organic Chemistry, Russian Academy of Sciences, Leninsky Prosp., 47, 119334 Moscow, Russia

<sup>4</sup> Departament de Química, Universitat de les Illes Balears, Crta de Valldemossa Km 7.5, 07122 Palma de Mallorca, Spain

\* Correspondence: tskhovrebov-ag@rudn.ru

**Abstract:** The series of substituted 1,2,4-selenodiazolium tetraphenylborate complexes were synthesized via cyclization between 2-pyridylselenenylchloride, followed by the anion metathesis, and fully characterized. The utilization of tetraphenylborate anion, a strong  $\pi$ -electron donor via its phenyl rings, promoted the formation of assemblies exhibiting selenium– $\pi$  interactions. The chalcogen bonding (ChB) interactions involving the  $\pi$ -systems of the tetraphenylborate anion were studied using density functional theory (DFT) calculations, where “mutated” anions were used to estimate the strength of the Se··· $\pi$  chalcogen bonds. Moreover, molecular electrostatic potential (MEP) surfaces were used to investigate the electron-rich and poor regions of the ion pairs. The quantum theory of atoms-in-molecules (QTAIM) and the noncovalent interaction (NCI) plot methods based on the topology of the electron density were used and combined to characterize the ChBs. The investigation reported herein disclosed that the formation of symmetrical dimers can be broken by the introduction of a stronger  $\pi$ -acceptor and, consequently, forming stronger Se··· $\pi$  contacts with selenodiazolium cations.

**Keywords:** selenium– $\pi$  interactions; noncovalent interactions; chalcogen heterocycles; chalcogen bonding



**Citation:** Sapronov, A.A.; Kubasov, A.S.; Khrustalev, V.N.; Artemjev, A.A.; Burkin, G.M.; Dukhnovsky, E.A.; Chizhov, A.O.; Kritchenkov, A.S.; Gomila, R.M.; Frontera, A.; et al. Se··· $\pi$  Chalcogen Bonding in 1,2,4-Selenodiazolium Tetraphenylborate Complexes. *Symmetry* **2023**, *15*, 212. <https://doi.org/10.3390/sym15010212>

Academic Editors: Sergei D. Odintsov and Enrico Bodo

Received: 14 December 2022

Revised: 27 December 2022

Accepted: 9 January 2023

Published: 11 January 2023



**Copyright:** © 2023 by the authors. Licensee MDPI, Basel, Switzerland. This article is an open access article distributed under the terms and conditions of the Creative Commons Attribution (CC BY) license (<https://creativecommons.org/licenses/by/4.0/>).

## 1. Introduction

Chalcogen bonding (ChB) is a noncovalent interaction where the chalcogen atom acts as an acceptor of electron density from an electronegative atom [1–4]. It is similar to a classical case of hydrogen bonding (HB), which is widely applied for the creation of supramolecular assemblies and extended structures (i.e., supramolecular organic frameworks (SOFs)) [5,6]. In contrast to HB, ChB has not yet received much attention in the creation of extended structures, although ChB is characterized by a remarkable directional-ity and strength tunability.

Recently, we discovered novel selenodiazolium salts, which were shown to be able to act as a donor of chalcogen bonds [7–10]. In some instances, the cations formed Se<sub>2</sub>N<sub>2</sub> squares via two antiparallel Se···N ChB, which potentially could be employed as nodes for the creation of extended supramolecular structures [7–10]. However, the squares' formation was not reliable and was dependent on the substituents in the selenodiazolium core. Thus, other noncovalent interactions could be more significant, outcompete Se<sub>2</sub>N<sub>2</sub> squares formation, and define the packing preference. This stimulated us to search for strategies that could allow us to form Se<sub>2</sub>N<sub>2</sub> squares in a rational way. In our recent study,

we demonstrated that 1,2,4-selenodiazolium salts, carrying benzylic substituents, with weakly binding anions reliably formed supramolecular dimers featuring four center  $\text{Se}_2\text{N}_2$  ChB and two selenium–arene interactions [10].

Following our interest in non-covalent interactions and chalcogen heterocycles [11–15], here we demonstrate that the symmetrical dimers could be broken by the introduction of  $\text{BPh}_4^-$  anion, which is a stronger acceptor of ChB and forms stronger  $\text{Se}\cdots\pi$  contacts with selenodiazolium cations. This shows that one arene could be predictably substituted by the other one in the ChB interaction pair, if this arene is a stronger electron donor. The strength of the  $\text{Se}\cdots\pi$  interactions has been evaluated using density functional theory (DFT) calculations. Computational methods are convenient not only to evaluate the energetic features of the ChB contacts, but also to investigate the physical nature of the interaction using several computational tools based on the analysis of the electron density. Moreover, the molecular electrostatic potential (MEP) surface method allows the identification of the  $\sigma$ -holes and their intensity. It is useful, especially in ChBs where two different  $\sigma$ -holes may exist, in order to analyze the competition between them and rationalize the supramolecular assemblies observed in the solid state.

## 2. Results and Discussion

Initial 1,2,4-selenodiazolium chlorides **1–4** were simply prepared in 85–93% yields according to our method [7,10]. Compound **2** was recrystallized from  $\text{CH}_2\text{Cl}_2$  to give a single crystal, which was analyzed by the X-ray structural analysis, which showed that **2** forms  $\text{Se}_2\text{N}_2$  squares in the solid form—the structural motif, which is typical for 1,2,4-selenodiazolium chlorides (Figure 1).

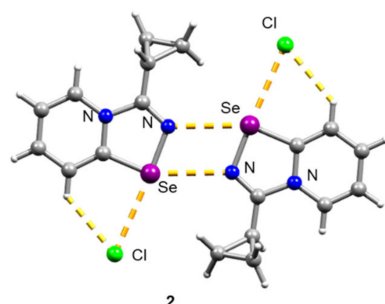
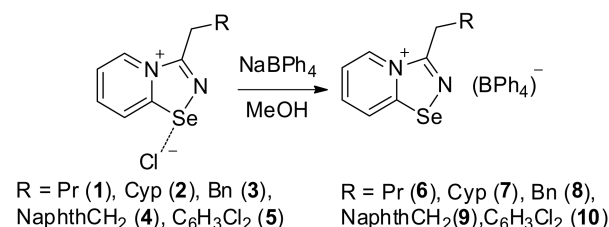


**Figure 1.** Ball-and-stick representation of the X-ray structure of **2**. Grey and light-grey spheres represent carbon and hydrogen, correspondingly.

The addition of the saturated MeOH solution of sodium tetraphenylborate to the solution of **1–4** in MeOH resulted in the precipitation of microcrystalline solids of **5–8** (Scheme 1). Isolation and analysis of the solids (see Supplementary Materials) suggested the formation of  $\text{BPh}_4^-$  salts **5–8** in high yields.



**Scheme 1.** Synthesis of **6–10**.

Crystals suitable for X-ray structural analysis were obtained by the recrystallization of **6–10** in MeOH (Figure 2). The N–Se and C=N separations are typical for the N–Se single and C=N double bonds [16–18].

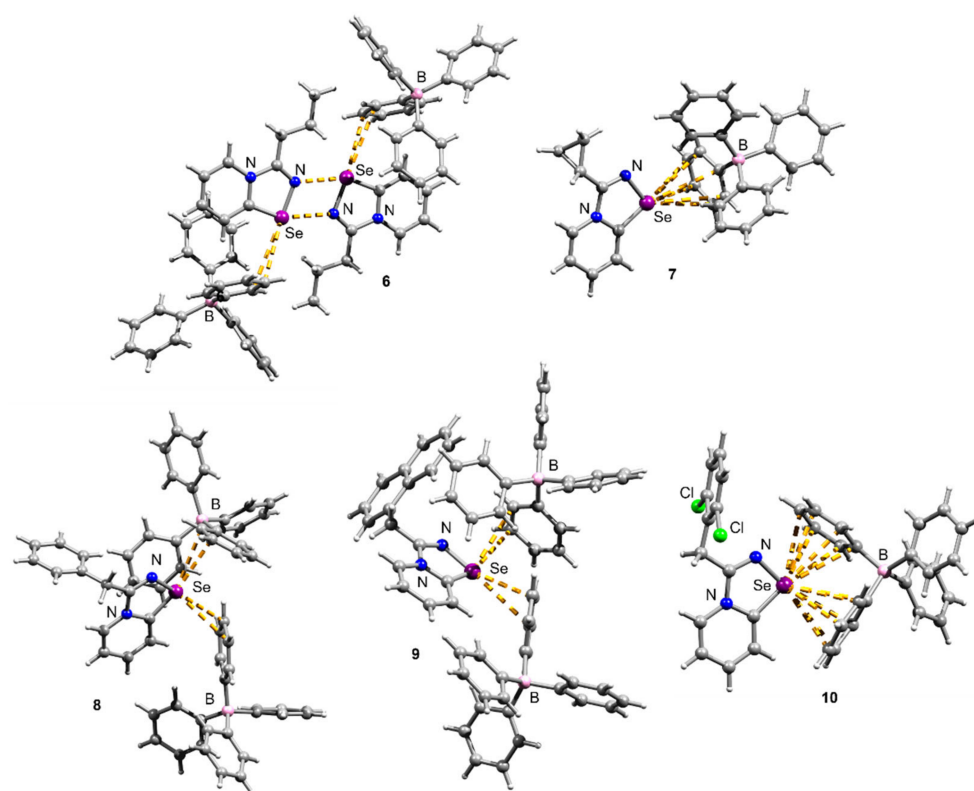


**Figure 2.** Ball-and-stick representations of the X-ray structures of **6–10**. Grey and light-grey spheres represent carbon and hydrogen, correspondingly.

Compounds **6–10** featured multiple  $\text{Se}\cdots\pi$  ChB contacts in the solid state; however, the geometry of  $\text{Se}\cdots\pi$  interactions was slightly different in all the cases. It should be noted that  $\text{Se}\cdots\pi$  interactions are relatively rare, although  $\text{S}\cdots\pi$  contacts are better documented [17,18].

Interestingly, the Pr-substituted selenodiazolium salt **6** unexpectedly formed the  $\text{Se}_2\text{N}_2$  square when the Cl anion was replaced by the  $\text{BPh}_4$  (Figure 2). The chloride **1** self-assembles into one-dimensional supramolecular polymers via  $\text{Se}\cdots\text{Cl}$  and  $\text{H}\cdots\text{Cl}$  interactions in the crystal [8]. This behavior of the Pr-substituted salt was unexpected; so far, we have observed the destruction of the  $\text{Se}_2\text{N}_2$  square on the  $\text{BPh}_4$  addition. For **6**  $\text{BPh}_4$  anion interacted with the cation via  $\text{Se}\cdots\pi$  ChB.

In contrast, the Cyp-substituted compound **7** showed no  $\text{Se}_2\text{N}_2$  square formation (Figure 2), while **2** formed a dimer in the solid state (Figure 1). The situation here was opposite to what we observed for the Pr-substituted derivative. The Se atom in **7** interacted with the  $\text{BPh}_4$  anion via  $\text{Se}\cdots\text{Ph}$  ChB (Figure 2).

The Bn and  $\text{CH}_2\text{Naphth}$  derivatives **8** and **9** also did not form  $\text{Se}_2\text{N}_2$  squares in the solid state (Figure 2), and this was expected. Earlier we showed that the replacement of the chloride by weakly binding anions invoked the formation of supramolecular dimers showing  $\text{Se}_2\text{N}_2$  squares with two  $\text{Se}\cdots\pi$  interactions [10]. The replacement of the Cl by the  $\text{BPh}_4$  expectedly did not result in the formation of  $\text{Se}_2\text{N}_2$  squares since  $\text{Se}\cdots\pi$  ChB with the  $\text{BPh}_4$  is stronger than with the neutral aryl of the selenodiazolium cation.

Finally, compound **10** also featured  $\text{Se}\cdots\pi$  ChB with the  $\text{BPh}_4$ ; however, in contrast to the previous cases, the Se atom interacted with two  $\text{BPh}_4$  anions in a  $\eta^6$  fashion (Figure 2).

For the Cyp selenodiazolium derivative **11** with  $\text{AuCl}_4$  anion, we also managed to obtain single crystals and characterize them by means of the X-ray structural analysis (Figure 3). The addition of  $\text{NaAuCl}_4$  to **2** in MeOH resulted in the formation of a microcrystalline precipitate of **11** (Scheme 2). Isolation and analysis of the solids (see SI) suggested the formation of  $\text{AuCl}_4$  salt.

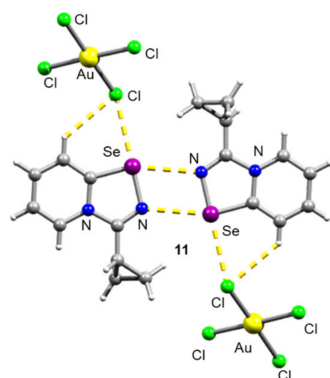
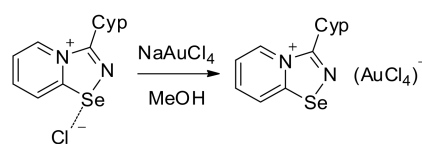


**Figure 3.** Ball-and-stick representation of the X-ray structure of **11**. Grey and light-grey spheres represent carbon and hydrogen, respectively.



**Scheme 2.** Synthesis of **11**.

The structural analysis revealed that **11** also featured form  $\text{Se}_2\text{N}_2$  squares in the solid state (Figure 1). A weakly binding  $\text{AuCl}_4^-$  anion did not invoke the square rupture in contrast to the  $\text{BPh}_4^-$ .

In order to better understand the  $\text{Se} \cdots \pi$  ChB in **7–10**, we carried out density functional theory (DFT) studies. As a starting point, the molecular electrostatic potential (MEP) surfaces of the anion and two selenodiazolium cations (Cyp and Bn-substituted) were computed. The MEP surfaces are plotted in Figure 3, along with the values at the phenyl rings of the anion and both  $\sigma$ -holes of the selenium atom. Regarding the anion, the MEP surface reveals that the MEP minimum is located in the region under the influence of two phenyl rings of the anion ( $-103$  kcal/mol) see Figure 4a. The MEP is less negative at the opposite side of the phenyl rings  $-89$  kcal/mol. In both cations, the deeper  $\sigma$ -hole ( $124$  kcal/mol) is found to be the opposite to the N–Se due to the overlap with the positive and adjacent H-atom of the pyridyl ring (see Figure 4b,c). The MEP value at the other  $\sigma$ -hole (opposite to C–Se bond) is almost identical in both cations and around  $25$  kcal/mol less positive than that opposite to the N–Se bond.

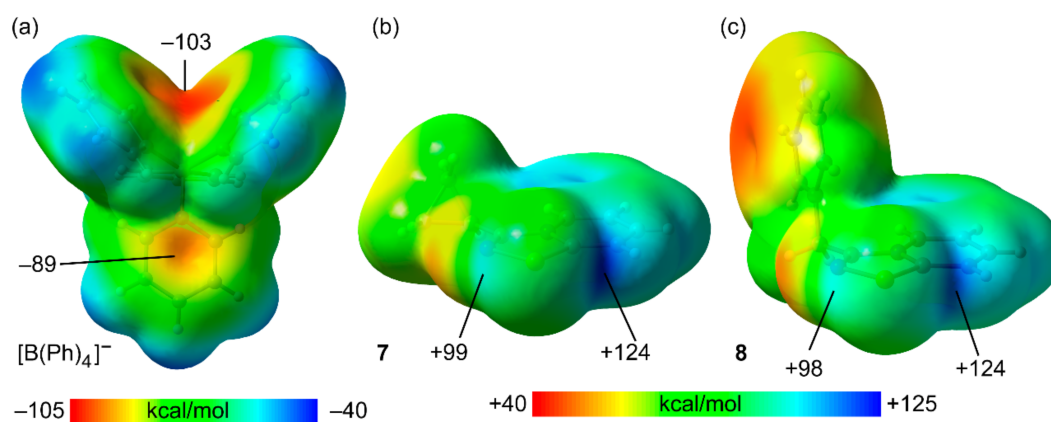


**Figure 4.** MEP surfaces of compound the tetraphenylborate (a), and the cationic units of compounds **7** (b) and **8** (c) at the PBE0-D3/def2-TZVP level of theory. Values in kcal/mol.

The QTAIM and NCIplot analyses combined in the same plot of the  $\text{Se} \cdots \pi$  ion-pair dimers of compounds **7–10** are shown in Figure 5, accompanied by the interaction energies.

For simplicity, only intermolecular interactions are represented in the QTAIM and NCI plots. In Figure 5, the bond critical points (CPs) are represented as red spheres, and bond paths are represented as orange lines. The reduced density gradient (RDG) isosurfaces ( $s = 0.45$ ) are overlapped with the QTAIM analysis. Remarkably, the existence of the  $\text{Se}\cdots\pi$  ChBs in all ion-pair dimers is confirmed by both QTAIM and NCIplot analyses. The QTAIM analysis shows the existence of only one bond CP and bond path connecting the Se-atom to one carbon atom of the phenyl ring. The  $\text{Se}\cdots\pi$  nature of the interaction is better described by the NCIplot analysis. That is, the shape and extension of the RDG isosurfaces in all compounds are typical of  $\pi$ -interactions as they embrace most of the  $\pi$ -cloud of the aromatic rings. The interaction energies range from  $-54.6$  kcal/mol in **7** to  $-65.6$  kcal/mol in compound **10**. These large interaction energies are due to the ion-pair nature of the dimers; that is, the existence of strong and non-directional coulombic forces. The QTAIM and NCIplot analyses also disclose the existence of additional contacts with other parts of the anion, which are  $\text{CH}\cdots\text{N,Se}$  H-bonds in **7**,  $\pi(\text{phenyl})\cdots\pi(\text{selenodiazolium})$  interactions in **8** and **9**, and  $\text{CH}\cdots\text{Cl}$  H-bond in **10**, all of them characterized by the corresponding bond CPs and green RDG isosurfaces. In an effort to estimate the relative contribution of the  $\text{Se}\cdots\pi$  interaction without the participation of the strong coulombic forces and rest of the contacts, we have computed the dimerization energies using modified dimers. The modification consists of the replacement of the interacting phenyl ring of the anion by a hydrogen atom. As a consequence, the  $\text{Se}\cdots\pi$  interaction in the ion-pair dimers is not established but the coulombic force is maintained, as well as the contacts with the other phenyl. In the modified dimers, the interaction energies are moderately reduced (see values at the bottom of Figure 5). The energy differences between the unmodified and mutated dimers correspond to a rough estimation of the  $\text{Se}\cdots\pi$  energies, which range from  $-7.3$  kcal/mol in **9** to  $-11.1$  kcal/mol in **7**. For compound **10**, where two  $\text{Se}\cdots\pi$  interactions are established, we have computed two mutated dimers by replacing either the phenyl group labeled A or the one labeled B with an H-atom (see Figure 5d). The  $\text{Se}\cdots\pi$  energies are  $-7.3$  kcal/mol for the phenyl A and  $-10.4$  kcal/mol for phenyl B, in line with the relative intensity of the  $\sigma$ -holes opposite to C–Se, and N–Se disclosed by the MEP surface analysis.

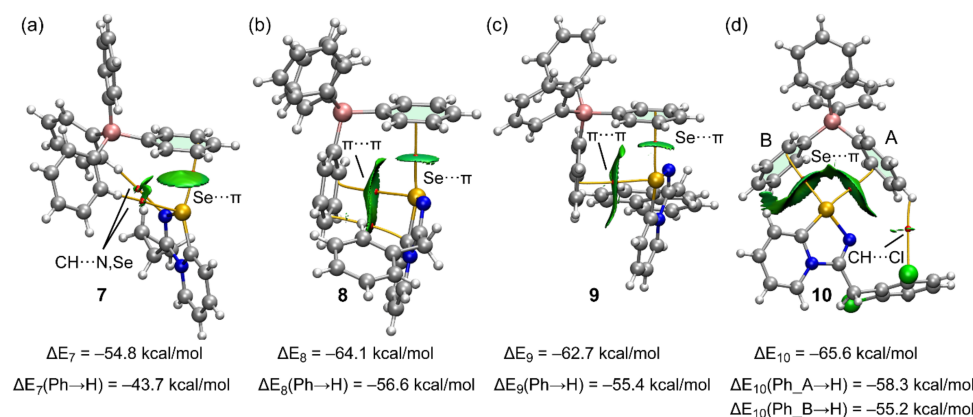


**Figure 5.** Combined QTAIM (CPs in red and bond paths as orange lines) and NCIplot analyses of the ion pair dimers of **7** (a) **8** (b), **9** (c), and **10** (d). The ion-pair energies using the X-ray geometries and the modified dimers are also indicated. Isovalue for the RDG isosurface 0.45.

### 3. Materials and Methods

**Computational details.** The calculations of the ion pair dimers of compounds **7–10** were performed using the Turbomole 7.2 program [19] and the X-ray coordinates. Consequently, vibrational analysis was not performed. The PBE0-D3/def2-TZVP [20–23] level of theory was used as it has been successfully used for studying similar interactions. The default convergence criterion was used for the calculations. The MEP surfaces were constructed using the 0.001 a.u. isosurface and the same level of theory. The QTAIM [24] distribution of CPs and bond paths, and NCIplot RDG isosurfaces [25] were plotted using the VMD

program [26]. The following settings were used for the RDG plots:  $s = 0.45$  a.u.; cut-off  $\rho = 0.04$  a.u.; color scale  $-0.025$  a.u.  $\leq \text{sign}(\lambda_2)\rho \leq 0.025$  a.u.

#### Synthetic part.

Di(2-pyridyl)diselenide was prepared as reported earlier [10].

**Synthesis of 2.** The 2-Pyridylselenyl chloride (129  $\mu\text{mol}$ , 25 mg) was suspended in  $\text{CH}_2\text{Cl}_2$  (3 mL), then cyanocyclopropane (100  $\mu\text{L}$ ) was added and the mixture was stirred at room temperature for 5 h. Colorless precipitate formed was filtered and dried under vacuum. Yield: 29 mg (85%).  $^1\text{H}$  NMR (600 MHz,  $\text{D}_2\text{O}$ )  $\delta$  9.69 (d,  $J = 6.5$  Hz, 1H, H5), 8.79 (d,  $J = 8.5$  Hz, 1H, H8), 8.41 (t,  $J = 7.7$  Hz, 1H, H7), 8.05 (t,  $J = 6.7$  Hz, 1H, H6), 2.64–2.50 (m, 1H, CH), 1.45–1.22 (m, 4H,  $\text{CH}_2$ ).  $^{13}\text{C}$  NMR (151 MHz,  $\text{D}_2\text{O}$ )  $\delta$  167.80 (C3), 159.60 (C9), 139.61 (C5), 136.28 (C8), 125.74 (C7), 122.89 (C6), 10.93 (CH), 6.63 ( $\text{CH}_2$ ). MS (ESI<sup>+</sup>), found: 224.9925 [M–Cl]<sup>+</sup>; calcd for  $\text{C}_9\text{H}_9\text{N}_2\text{Se}$ : 224.9926.

**Synthesis of 6.** The 2-Pyridylselenyl chloride (119  $\mu\text{mol}$ , 23 mg) was suspended in  $\text{CH}_2\text{Cl}_2$  (3 mL), then PrCN (100  $\mu\text{L}$ ) was added, and the mixture was stirred at room temperature for 24 h.  $\text{Et}_2\text{O}$  (2 mL) was added, and the colorless precipitate was filtered, dried under vacuum, and redissolved in MeOH (4 mL). Addition of the saturated MeOH solution of  $\text{NaBPh}_4$  (100  $\mu\text{L}$ ) resulted in the formation of microcrystalline precipitate. Yield: 54 mg (84%).  $^1\text{H}$  NMR (600 MHz,  $\text{Me}_2\text{CO}-d_6$ )  $\delta$  9.40 (d,  $J = 6.8$  Hz, 1H, H5), 9.00 (d,  $J = 8.6$  Hz, 1H, H8), 8.45 (td,  $J = 8.4$  Hz, 1H, H7), 8.05 (td,  $J = 6.9$  Hz, 1H, H6), 7.35 (m,  $J = 6.5$  Hz, 8H), 6.91 (t,  $J = 7.4$  Hz, 8H), 6.79–6.73 (t, 4H), 3.31 (t,  $J = 7.3$  Hz, 2H), 2.83 (s, 2H), 1.14 (t,  $J = 7.4$  Hz, 3H).

**Synthesis of 7.** The 2-Pyridylselenyl chloride (78  $\mu\text{mol}$ , 15 mg) was suspended in  $\text{CH}_2\text{Cl}_2$  (3 mL), then cyanocyclopropane (100  $\mu\text{L}$ ) was added, and the mixture was stirred at room temperature for 5 h. Colorless precipitate formed was filtered, dried under vacuum, and redissolved in MeOH (4 mL). Addition of the saturated MeOH solution of  $\text{NaBPh}_4$  (100  $\mu\text{L}$ ) resulted in the formation of yellow microcrystalline precipitate. Yield: 36 mg (86%).  $^1\text{H}$  NMR (600 MHz,  $\text{Me}_2\text{CO}-d_6$ )  $\delta$  9.65 (d,  $J = 6.7$  Hz, 1H, H5), 8.92 (d,  $J = 8.6$  Hz, 1H, H8), 8.39 (td,  $J = 7.9$  Hz, 1H, H7), 8.01 (td,  $J = 7.0$  Hz, 1H, H6), 7.37–7.31 (m, 8H), 6.91 (t,  $J = 7.4$  Hz, 8H), 6.76 (t,  $J = 7.5$  Hz, 4H), 1.38–1.27 (m, 5H). MS (ESI<sup>+</sup>), found: 224.9925 [M–BPh<sub>4</sub>]<sup>+</sup>; calcd for  $\text{C}_9\text{H}_9\text{N}_2\text{Se}$ : 224.9926.

**Synthesis of 8.** The 2-Pyridylselenyl chloride (93  $\mu\text{mol}$ , 18 mg) was suspended in phenylacetonitrile (1 mL) and the mixture was stirred at room temperature for 24 h. Yellow precipitate formed was filtered, dried under vacuum, and redissolved in MeOH (3 mL). Addition of the saturated MeOH solution of  $\text{NaBPh}_4$  (100  $\mu\text{L}$ ) resulted in the formation of microcrystalline precipitate. Yield: 31 mg (81%).  $^1\text{H}$  NMR (600 MHz,  $\text{CD}_2\text{Cl}_2$ )  $\delta$  10.79 (d,  $J = 6.8$  Hz, 1H), 10.68–10.52 (m, 10H), 10.35 (m,  $J = 6.8$  Hz, 3H), 10.26 (d,  $J = 7.0$  Hz, 1H), 10.09 (t,  $J = 7.5$  Hz, 8H), 9.90 (t,  $J = 7.2$  Hz, 4H), 8.67–8.32 (t, 1H), 7.17 (s, 2H), 4.74 (s, 2H). MS (ESI<sup>+</sup>), found: 275.0082 [M–BPh<sub>4</sub>]<sup>+</sup>; calcd for  $\text{C}_{13}\text{H}_{11}\text{N}_2\text{Se}$ : 275.0082.

**Synthesis of 9.** The 2-Pyridylselenyl chloride (68  $\mu\text{mol}$ , 13 mg) was suspended in  $\text{CH}_2\text{Cl}_2$  (2 mL) and MeOH (2 mL), then 1-naphthacetonitrile (50 mg) was added and the solution was stirred at room temperature for 4 h. Addition of  $\text{Et}_2\text{O}$  is result of colorless precipitate formed was filtered, dried under vacuum, and redissolved in MeOH (4 mL). Addition of the saturated MeOH solution of  $\text{NaBPh}_4$  (100  $\mu\text{L}$ ) resulted in the formation of microcrystalline precipitate. Yield: 33 mg (78%). Anal. Calcd:  $\text{C}_{41}\text{H}_{33}\text{BN}_2\text{Se}$ : C, 76.53; H, 5.17; B, 1.68; N, 4.35; Se, 12.27.  $^1\text{H}$  NMR (600 MHz,  $\text{CD}_2\text{Cl}_2$ )  $\delta$  11.50 (d,  $J = 6.7$  Hz, 1H), 11.00 (d,  $J = 7.3$  Hz, 1H), 10.68–10.56 (m, 14H), 10.14 (t,  $J = 7.4$  Hz, 8H), 9.97 (t,  $J = 7.2$  Hz, 4H), 8.54–8.50 (s, 5H). MS (ESI<sup>+</sup>), found: 325.0237 [M–BPh<sub>4</sub>]<sup>+</sup>; calcd for  $\text{C}_{17}\text{H}_{13}\text{N}_2\text{Se}$ : 325.0238.

**Synthesis of 10.** The solution of  $\text{PhICl}_2$  (13.4 mg, 0.05 mmol) and 2-(2,6-dichlorophenyl) acetonitrile (50 mg) in  $\text{CH}_2\text{Cl}_2$  (3 mL) was added to 2,2'-dipyridyldiselenide (15.5 mg, 0.05 mmol) in  $\text{CH}_2\text{Cl}_2$  (1 mL), and the reaction mixture was left without stirring for 5 h. After that a solution was decanted from yellow crystalline precipitate, which was washed with  $\text{Et}_2\text{O}$  ( $3 \times 1$  mL) and dried under vacuum. Addition of the MeOH solution (100  $\mu\text{L}$ ) of  $\text{NaBPh}_4$  (50 mg) to MeOH solution of **5** (1 mL) resulted in the formation of microcrystalline precipitate. Yield: 42 mg (63%).  $^1\text{H}$  NMR (600 MHz,  $\text{Me}_2\text{CO}-d_6$ )  $\delta$  9.82 (d,  $J = 6.8$  Hz, 1H,

H5), 9.07 (d,  $J = 8.6$  Hz, 1H, H8), 8.53 (td,  $J = 8.4$  Hz, 1H, H7), 8.19 (td,  $J = 7.0$  Hz, 1H, H6), 7.65–7.47 (m, 3H), 7.35 (m,  $J = 6.7$  Hz, 8H), 6.92 (t,  $J = 7.4$  Hz, 8H), 6.81–6.71 (t,  $J = 7.2$  Hz, 4H), 5.12 (s, 2H).

**Synthesis of 11.** The 2-Pyridylselenenyl chloride (83  $\mu\text{mol}$ , 16 mg) was suspended in  $\text{CH}_2\text{Cl}_2$  (3 mL), then cyanocyclopropane (100  $\mu\text{L}$ ) was added, and the mixture was stirred at room temperature for 5 h. Colorless precipitate formed was filtered, dried under vacuum, and redissolved in MeOH (4 mL). Addition of the saturated MeOH solution of  $\text{NaAuCl}_4$  (100  $\mu\text{L}$ ) resulted in the formation of yellow microcrystalline precipitate. Yield: 24 mg (52%).  $^1\text{H}$  NMR (600 MHz,  $\text{Me}_2\text{CO}-d_6$ )  $\delta$  9.99 (d,  $J = 6.8$ , 1.0 Hz, 1H, H5), 9.15 (d,  $J = 8.6$  Hz, 1H, H8), 8.61 (td,  $J = 7.9$  Hz, 1H, H7), 8.26 (td,  $J = 7.0$  Hz, 1H, H6), 1.44–1.34 (m, 4H), 1.06–0.96 (m, 1H).  $^{13}\text{C}$  NMR (151 MHz,  $\text{Me}_2\text{CO}-d_6$ )  $\delta$  139.84, 136.97, 126.52, 123.26, 11.29, 7.06.

#### 4. Conclusions

We have synthesized a series of benzylic-substituted 1,2,4-selenodiazolium tetraphenylborates exhibiting  $\text{Se}\cdots\pi$  interactions. We showed that the symmetrical dimers could be broken by the introduction of the  $\text{BPh}_4$  anion. This demonstrates that one arene could be predictably substituted by the other one in the ChB interaction pair if this arene is a stronger electron donor. The DFT study demonstrates that the  $\text{Se}-\pi$  interaction energies are moderately strong, ranging from  $-11$  to  $-7$  kcal/mol, due to the participation of the electron-rich aromatic surface of the anion as an electron donor. The  $\text{Se}\cdots\pi$  interactions described in this work have been further characterized by the QTAIM and NCIPLOT methodologies, both based on the topology of the electron density. The latter describes better the  $\pi$ -nature of the interaction by means of the RDG isosurfaces that represent the contact in real space.

**Supplementary Materials:** The following are available online at: <https://www.mdpi.com/article/10.3390/sym15010212/s1>, X-ray crystal structure determination [27–31]. Table S1. Crystal data and structure refinement for all compounds studied.

**Author Contributions:** Conceptualization, A.G.T.; methodology, A.S.K. (Andrei S. Kritchenkov); investigation, A.A.S., A.A.A., V.N.K., A.S.K. (Alexey S. Kubasov), R.M.G., G.M.B., E.A.D. and A.O.C.; writing—original draft preparation, A.F. and A.G.T. All authors have read and agreed to the published version of the manuscript.

**Funding:** This work was performed under the support of the Russian Science Foundation (award No. 22-73-10007). Theoretical investigations were funded by the “Ministerio de Ciencia, Investigación y Universidades/Agencia Estatal de Investigación” (MICIU/AEI/10.13039/501100011033) of Spain (project PID2020-115637GB-I00, FEDER funds). X-ray structural analysis was performed under the support of Ministry of Education and Science of the Russian Federation (award No. 075-03-2020-223 (FSSF-2020-0017)).

**Conflicts of Interest:** The authors declare no conflict of interest.

#### References

1. Wang, W.; Ji, B.; Zhang, Y. Chalcogen Bond: A Sister Noncovalent Bond to Halogen Bond. *J. Phys. Chem. A* **2009**, *113*, 8132–8135. [[CrossRef](#)] [[PubMed](#)]
2. Pascoe, D.J.; Ling, K.B.; Cockroft, S.L. The Origin of Chalcogen-Bonding Interactions. *J. Am. Chem. Soc.* **2017**, *139*, 15160–15167. [[CrossRef](#)]
3. Bortoli, M.; Ahmad, S.M.; Hamlin, T.A.; Bickelhaupt, F.M.; Orian, L. Nature and strength of chalcogen– $\pi$  bonds. *Phys. Chem. Chem. Phys.* **2018**, *20*, 27592–27599. [[CrossRef](#)] [[PubMed](#)]
4. Aakeroy, C.B.; Bryce, D.L.; Desiraju, G.R.; Frontera, A.; Legon, A.C.; Nicotra, F.; Rissanen, K.; Scheiner, S.; Terraneo, G.; Metrangolo, P.; et al. Definition of the chalcogen bond (IUPAC Recommendations 2019). *Pure Appl. Chem.* **2019**, *91*, 1889–1892. [[CrossRef](#)]
5. Slater, A.G.; Cooper, A.I. Function-led design of new porous materials. *Science* **2015**, *348*, aaa8075. [[CrossRef](#)] [[PubMed](#)]
6. Wang, B.; Lin, R.-B.; Zhang, Z.; Xiang, S.; Chen, B. Hydrogen-Bonded Organic Frameworks as a Tunable Platform for Functional Materials. *J. Am. Chem. Soc.* **2020**, *142*, 14399–14416. [[CrossRef](#)]

7. Khrustalev, V.N.; Grishina, M.M.; Matsulevich, Z.V.; Lukiyanova, J.M.; Borisova, G.N.; Osmanov, V.K.; Novikov, A.S.; Kirichuk, A.A.; Borisov, A.V.; Solari, E.; et al. Novel cationic 1,2,4-selenodiazoles: Synthesis via addition of 2-pyridylselenenyl halides to unactivated nitriles, structures and four-center Se···N contacts. *Dalt. Trans.* **2021**, *50*, 10689–10691. [[CrossRef](#)]
8. Grudova, M.V.; Kubasov, A.S.; Khrustalev, V.N.; Novikov, A.S.; Kritchenkov, A.S.; Nenajdenko, V.G.; Borisov, A.V.; Tskhovrebov, A.G. Exploring Supramolecular Assembly Space of Cationic 1,2,4-Selenodiazoles: Effect of the Substituent at the Carbon Atom and Anions. *Molecules* **2022**, *27*, 1029. [[CrossRef](#)]
9. Artemjev, A.A.; Novikov, A.P.; Burkin, G.M.; Sapronov, A.A.; Kubasov, A.S.; Nenajdenko, V.G.; Khrustalev, V.N.; Borisov, A.V.; Kirichuk, A.A.; Kritchenkov, A.S.; et al. Towards Anion Recognition and Precipitation with Water-Soluble 1,2,4-Selenodiazolium Salts: Combined Structural and Theoretical Study. *Int. J. Mol. Sci.* **2022**, *23*, 6372. [[CrossRef](#)]
10. Sapronov, A.A.; Artemjev, A.A.; Burkin, G.M.; Khrustalev, V.N.; Kubasov, A.S.; Nenajdenko, V.G.; Gomila, R.M.; Frontera, A.; Kritchenkov, A.S.; Tskhovrebov, A.G. Robust Supramolecular Dimers Derived from Benzylic-Substituted 1,2,4-Selenodiazolium Salts Featuring Selenium $\pi$ ; Chalcogen Bonding. *Int. J. Mol. Sci.* **2022**, *23*, 14973.
11. Repina, O.V.; Novikov, A.S.; Khoroshilova, O.V.; Kritchenkov, A.S.; Vasin, A.A.; Tskhovrebov, A.G. Lasagna-like supramolecular polymers derived from the PdII osazone complexes via C(sp<sup>2</sup>)-H···Hal hydrogen bonding. *Inorganica Chim. Acta* **2020**, *502*, 119378. [[CrossRef](#)]
12. Tskhovrebov, A.G.; Novikov, A.S.; Tupertsev, B.S.; Nazarov, A.A.; Antonets, A.A.; Astafiev, A.A.; Kritchenkov, A.S.; Kubasov, A.S.; Nenajdenko, V.G.; Khrustalev, V.N. Azimidazole Gold(III) Complexes: Synthesis, Structural Characterization and Self-Assembly in the Solid State. *Inorg. Chim. Acta* **2021**, *522*, 120373. [[CrossRef](#)]
13. Tskhovrebov, A.G.; Novikov, A.S.; Kritchenkov, A.S.; Khrustalev, V.N.; Haukka, M. Attractive halogen···halogen interactions in crystal structure of trans-dibromogold(III) complex. *Z. Krist.-Cryst. Mater.* **2020**, *235*, 477–480. [[CrossRef](#)]
14. Shikhaliyev, N.G.; Maharramov, A.M.; Bagirova, K.N.; Suleymanova, G.T.; Tsyrenova, B.D.; Nenajdenko, V.G.; Novikov, A.S.; Khrustalev, V.N.; Tskhovrebov, A.G. Supramolecular organic frameworks derived from bromoaryl-substituted dichlorodiazabutadienes via Cl···Br halogen bonding. *Mendeleev. Commun.* **2021**, *31*, 191–193. [[CrossRef](#)]
15. Khrustalev, V.N.; Savchenko, A.O.; Zhukova, A.I.; Chernikova, N.Y.; Kurykin, M.A.; Novikov, A.S.; Tskhovrebov, A.G. Attractive fluorine···fluorine interactions between perfluorinated alkyl chains: A case of perfluorinated Cu(II) diiminate Cu[C<sub>2</sub>F<sub>5</sub>-C(NH)-CF=C(NH)-CF<sub>3</sub>]<sub>2</sub>. *Z. Krist.-Cryst. Mater.* **2021**, *236*, 117–122. [[CrossRef](#)]
16. Allen, F.H.; Kennard, O.; Watson, D.G.; Brammer, L.; Orpen, A.G.; Taylor, R. Tables of bond lengths determined by X-ray and neutron diffraction. Part 1. Bond lengths in organic compounds. *J. Chem. Soc. Perkin Trans. 2* **1987**, S1–S19. [[CrossRef](#)]
17. Nziko, V.d.P.N.; Scheiner, S. S $\pi$  Chalcogen Bonds between SF<sub>2</sub> or SF<sub>4</sub> and C–C Multiple Bonds. *J. Phys. Chem. A* **2015**, *119*, 5889–5897. [[CrossRef](#)]
18. Bhandary, S.; Sirohiwal, A.; Kadu, R.; Kumar, S.; Chopra, D. Dispersion Stabilized Se/Te $\pi$  Double Chalcogen Bonding Synthons in in Situ Cryocrystallized Divalent Organochalcogen Liquids. *Cryst. Growth Des.* **2018**, *18*, 3734–3739. [[CrossRef](#)]
19. Ahlrichs, R.; Bär, M.; Häser, M.; Horn, H.; Kölmel, C. Electronic structure calculations on workstation computers: The program system turbomole. *Chem. Phys. Lett.* **1989**, *162*, 165–169. [[CrossRef](#)]
20. Adamo, C.; Barone, V. Toward reliable density functional methods without adjustable parameters: The PBE0 model. *J. Chem. Phys.* **1999**, *110*, 6158–6170. [[CrossRef](#)]
21. Grimme, S.; Antony, J.; Ehrlich, S.; Krieg, H. A consistent and accurate ab initio parametrization of density functional dispersion correction (DFT-D) for the 94 elements H–Pu. *J. Chem. Phys.* **2010**, *132*, 154104. [[CrossRef](#)] [[PubMed](#)]
22. Weigend, F.; Ahlrichs, R. Balanced basis sets of split valence, triple zeta valence and quadruple zeta valence quality for H to Rn: Design and assessment of accuracy. *Phys. Chem. Chem. Phys.* **2005**, *7*, 3297. [[CrossRef](#)] [[PubMed](#)]
23. Weigend, F. Accurate Coulomb-fitting basis sets for H to Rn. *Phys. Chem. Chem. Phys.* **2006**, *8*, 1057–1065. [[CrossRef](#)] [[PubMed](#)]
24. Bader, R.F.W. A Quantum Theory of Molecular Structure and Its Applications. *Chem. Rev.* **1991**, *91*, 893–928. [[CrossRef](#)]
25. Contreras-García, J.; Johnson, E.R.; Keinan, S.; Chaudret, R.; Piquemal, J.-P.; Beratan, D.N.; Yang, W. NCIPLOT: A Program for Plotting Noncovalent Interaction Regions. *J. Chem. Theory Comput.* **2011**, *7*, 625–632. [[CrossRef](#)]
26. Humphrey, W.; Dalke, A.; Schulten, K. VMD: Visual molecular dynamics. *J. Mol. Graph.* **1996**, *14*, 33–38. [[CrossRef](#)]
27. Bruker. *SAINT*, v. 8.40A; Bruker AXS Inc.: Madison, Wisconsin, WI, USA, 2019.
28. Krause, L.; Herbst-Irmer, R.; Sheldrick, G.M.; Stalke, D. Comparison of Silver and Molybdenum Microfocus X-Ray Sources for Single-Crystal Structure Determination. *J. Appl. Cryst.* **2015**, *48*, 3–10. [[CrossRef](#)]
29. Rigaku. *CrysAlisPro Software System*, v. 1.171.41.106a; Rigaku: Oxford, UK, 2021.
30. Spek, A.L. *PLATON, A Multipurpose Crystallographic Tool*; Utrecht University: Utrecht, The Netherlands, 2015.
31. Sheldrick, G.M. Crystal Structure Refinement with It SHELXL. *Acta Cryst.* **2015**, *C71*, 3–8. [[CrossRef](#)]

**Disclaimer/Publisher’s Note:** The statements, opinions and data contained in all publications are solely those of the individual author(s) and contributor(s) and not of MDPI and/or the editor(s). MDPI and/or the editor(s) disclaim responsibility for any injury to people or property resulting from any ideas, methods, instructions or products referred to in the content.